J. Fluid Mech. (2024), *vol*. 999, R1, doi:10.1017/jfm.2024.995

On the boundary-layer asymmetry in two-dimensional annular Rayleigh–Bénard convection subject to radial gravity

Abhiroop Bhadra[1], **Olga Shishkina**[2] **and Xiaojue Zhu**[1,†]

[1]Max Planck Institute for Solar System Research, 37077 Göttingen, Germany

[2]Max Planck Institute for Dynamics and Self-Organization, 37077 Göttingen, Germany

(Received 12 September 2024; revised 8 October 2024; accepted 10 October 2024)

Radial unstable stratification is a potential source of turbulence in the cold regions of accretion disks. To investigate this thermal effect, here we focus on two-dimensional Rayleigh–Bénard convection in an annulus subject to radially dependent gravitational acceleration $g \propto 1/r$. Next to the Rayleigh number Ra and Prandtl number Pr, the radius ratio η, defined as the ratio of inner and outer cylinder radii, is a crucial parameter governing the flow dynamics. Using direct numerical simulations for $Pr = 1$ and Ra in the range from 10^7 to 10^{10}, we explore how variations in η influence the asymmetry in the flow field, particularly in the boundary layers. Our results show that in the studied parameter range, the flow is dominated by convective rolls and that the thermal boundary-layer (TBL) thickness ratio between the inner and outer boundaries varies as $\eta^{1/2}$. This scaling is attributed to the equality of velocity scales in the inner (u_i) and outer (u_o) regions. We further derive that the temperature drops in the inner and outer TBLs scale as $1/(1+\eta^{1/2})$ and $\eta^{1/2}/(1+\eta^{1/2})$, respectively. The scalings and the temperature drops are in perfect agreement with the numerical data.

Key words: turbulent convection, plumes/thermals, Bénard convection

1. Introduction

Thermal convection is a pivotal process in astrophysical and geophysical systems, critically influencing energy transport in a variety of environments. It drives the convective zones within stars (Hotta & Kusano 2021; Vasil, Julien & Featherstone 2021), shapes the interiors of planets (Samuel *et al.* 2021), governs atmospheric dynamics in gas giants (Christensen 2001; Christensen & Wicht 2008) and plays a significant role in the behaviour

† Email address for correspondence: zhux@mps.mpg.de

of protoplanetary disks (Klahr 2006; Hirose *et al.* 2014). Recent research has highlighted convection driven by radial stratification, with gravity pointing to the centre, as a potential driver of turbulence within the cold regions in protoplanetary disks, especially within the 1–10 AU range (Teed & Latter 2021). The cold regions inside protoplanetary disks, often modelled as cylindrical systems with central heating sources, present a unique challenge for understanding convection dynamics. To address this, our study employs two-dimensional (2-D) direct numerical simulations (DNS) within an annular geometry to investigate convection driven by radially dependent gravity, $g \propto 1/r$. While planar thermal convection, particularly Rayleigh–Bénard convection (RBC) between horizontal plates, has been extensively studied (Ahlers, Grossmann & Lohse 2009; Lohse & Xia 2010; Chillà & Schumacher 2012; Shishkina 2021; Lohse & Shishkina 2024), convection in annular configurations remains comparatively underexplored. Because of the relatively cheap computational cost, the 2-D simulations can provide valuable insights into annular RBC across a broad parameter space, advancing our understanding of the complex dynamics at play.

A key focus of this study is the asymmetry in thermal boundary-layer (TBL) thickness that arises in annular systems due to curvature effects. This asymmetry can significantly impact flow dynamics and heat transfer, making it essential for accurately characterizing convection processes. Our research examines these asymmetries using data from DNS, considering critical control parameters such as the Rayleigh number (Ra) and the Prandtl number (Pr). The radius ratio $\eta \equiv r_i/r_o$, where r_i and r_o are the inner and outer radii of the domain, respectively, serves as the primary geometric variable influencing the convection behaviour.

In comparison, previous studies have focused mainly on the boundary-layer (BL) asymmetry within the spherical shell convection (see Sharpe & Peltier 1978; Schubert & Zebib 1980; Zebib *et al.* 1983; Tilgner 1996). For instance, Jarvis (1993) attributed this asymmetry to differences in BL Rayleigh numbers (Ra_λ) for marginally stable BLs, following the criteria established by Malkus (1954). Extending this work, Vangelov & Jarvis (1994) explored 2-D axisymmetric convection and similarly observed TBL asymmetries, which they explained satisfactorily through the same marginal stability criteria. However, later work by Deschamps, Tackley & Nakagawa (2010) in spherical convection simulations challenged these findings. Their study revealed that the ratio of inner to outer Ra_λ scales as η^2, diverging from the previous assumption of equality. Notably, these earlier studies focused on simulating Earth's mantle conditions, assuming infinite Pr and a constant gravitational acceleration g. Recently, Gastine, Wicht & Aurnou (2015) conducted simulations of thermal convection in spherical geometries, with radius ratios η ranging from 0.2 to 0.95, Ra spanning from 10^3 to 10^9, and Pr fixed at 1. They explored various gravity profiles; including $g \propto r, 1, 1/r^2, 1/r^5$. Their results revealed that none of the previously established scaling arguments could adequately explain the asymmetry observed in their data. Instead, they proposed a new scaling argument based on the equality of interplume areas in the inner and outer shells, which explained the asymmetry. The only study that specifically addresses BL asymmetry in cylindrical geometry was conducted by Wang *et al.* (2022). In this work, they performed numerical simulations where a cold inner shell and a hot outer shell rotated coaxially, with centrifugal force serving as the buoyancy source. Their research explored a range of η from 0.3 to 0.9 and Ra from 10^6 to 10^8, using Pr of 4.3. To quantify the TBL asymmetry observed in their system, they employed the scaling methodology developed by Wu & Libchaber (1991) for non-Oberbeck–Boussinesq (NOB) RBC, providing valuable insights into the complexities of TBL behaviour in such configurations.

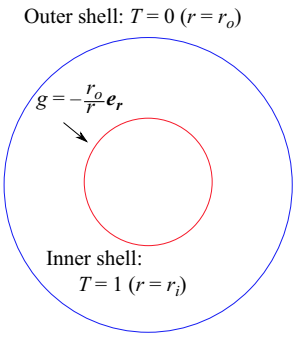

Figure 1. Sketch of the geometry used in the DNS with a hot inner shell at the inner radius r_i and a cold outer shell at the outer radius r_o.

The present study aims to quantify the asymmetry of TBL within a 2-D annular RBC system driven by radial gravity which is directed toward the centre and inversely proportional to the distance from the centre, as opposed to the centrifugal-force-driven convection explored by Wang *et al.* (2022). While previous studies have proposed various scaling laws for TBL asymmetry in different geometries, these scalings do not adequately describe the behaviour observed in our system. Therefore, the main motivation of this work is to derive new scaling laws tailored to this specific configuration, providing a more comprehensive understanding of the mechanisms driving TBL asymmetry in radially stratified convection systems.

2. Numerical model

The configuration considered in this study consists of a heated inner shell and a cooler outer shell, with radially inward gravity providing the buoyancy (see figure 1). This differs from set-ups that use the outward centrifugal force as the buoyancy source (see Jiang *et al.* 2020, 2022; Wang *et al.* 2022, 2023; Zhong, Wang & Sun 2023; Zhong, Li & Sun 2024; Yao *et al.* 2025) where the outer shell is heated and the inner shell is cooled. Since the considered gravitational acceleration equals $\boldsymbol{g} \equiv -g\boldsymbol{e_r}$, where $g \equiv r_o/r$ and $\boldsymbol{e_r}$ is the unit vector in the radial direction, the dimensionless equations governing the system are

$$\nabla \cdot \boldsymbol{u} = 0, \tag{2.1}$$

$$\frac{\partial \boldsymbol{u}}{\partial t} + \boldsymbol{u} \cdot \nabla \boldsymbol{u} = -\nabla p + \sqrt{\frac{Pr}{Ra}}\nabla^2 \boldsymbol{u} + gT\boldsymbol{e_r}, \tag{2.2}$$

$$\frac{\partial T}{\partial t} + \boldsymbol{u} \cdot \nabla T = \sqrt{\frac{1}{PrRa}}\nabla^2 T, \tag{2.3}$$

where $\boldsymbol{u}$, p, T and t denote the velocity, pressure, temperature and time, respectively. The control parameters include the Rayleigh number $Ra = \alpha g_o \Delta L^3/(\nu\kappa)$, the Prandtl number $Pr = \nu/\kappa$, and the radius ratio $\eta = r_i/r_o$. The non-dimensionalizing parameters are the characteristic length $L = r_o - r_i$, temperature $\Delta = T_i - T_o$, and free-fall velocity $U = \sqrt{\alpha g_o \Delta L}$. Here, α denotes the isobaric expansion coefficient, g_o is the gravitational constant at the outer shell, (ν) is the kinematic viscosity and (κ) is the thermal diffusivity while r_i and r_o are the inner and outer radii. We used a second-order finite-difference code, as referenced in Verzicco & Orlandi (1996), Van Der Poel *et al.* (2015) and Zhu *et al.* (2018*b*). All simulations enforce no-slip and isothermal boundary conditions.

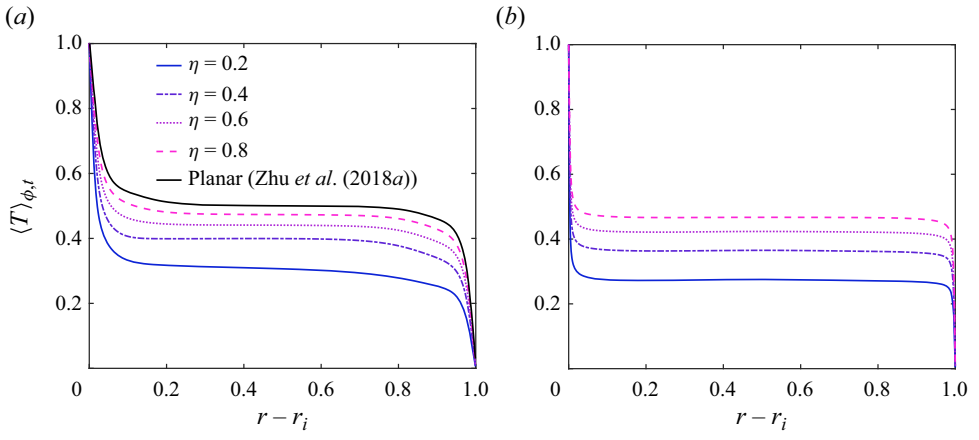

Figure 2. Azimuthally (ϕ) and temporally (t) averaged temperature fields for (a) $Ra = 10^7$ and (b) $Ra = 10^{10}$, and varying η. In (a), data from Zhu *et al.* (2018*a*) are added for comparison with planar RBC for the aspect ratio $\Gamma = 2$.

3. Flow field

In our simulations, Ra and η span from 10^7 to 10^{10} and 0.2 to 0.8, respectively. The averaged temperature fields, shown in figure 2, reveal that the midpoint temperature deviates from the average boundary temperatures, with this deviation becoming more pronounced at lower η. Additionally, the inner TBL width is smaller than the outer TBL width, with this asymmetry increasing as η decreases. Notably, for $Ra = 10^7$ at $\eta = 0.2$, a slight temperature gradient is observed in the bulk region of the flow.

Due to the 2-D nature of our simulations, the flow is dominated by convective rolls, as depicted in figure 3. These rolls are distorted by the flow geometry, becoming narrower near the inner shell and wider near the outer shell. At lower η, due to the increasing asymmetry in the flow field, the cold plume becomes fragmented. This is due to the shearing of the cold plume by the convective roll. Mass conservation requires any radially outward mass flux to be balanced by radial inflow. Since the plume widths scale with TBL widths (Ching *et al.* 2004), the radial flow velocity in the inner plume exceeds that in the outer plume. The convective rolls, driven by the hot inner plume, exhibit higher velocities compared with the outer plume. At lower η, this shear effect fragments the outer plume. This also causes cold fluid from the outer BL to be mixed into the bulk flow. Although higher Ra levels lead to increased mixing and temperature homogenization, at low η and low Ra (e.g. $\eta = 0.2$ and $Ra = 10^7$), the temperature gradient persists in the bulk region. As Ra increases, both inner and outer plumes break up, forming vortices that eventually merge into the convective rolls.

4. Boundary layers

For an annular geometry, the mismatch between the circumferences of the inner and outer shells leads to unequal heat fluxes through them. In our simulations, we have detected the BLs using the slope method, see e.g. Shishkina *et al.* (2010). Assuming purely conductive heat transfer through the TBLs, the following relation holds true in 2-D annular RBC:

$$\eta \frac{\Delta T_i}{\lambda_i} = \frac{\Delta T_o}{\lambda_o}, \tag{4.1}$$

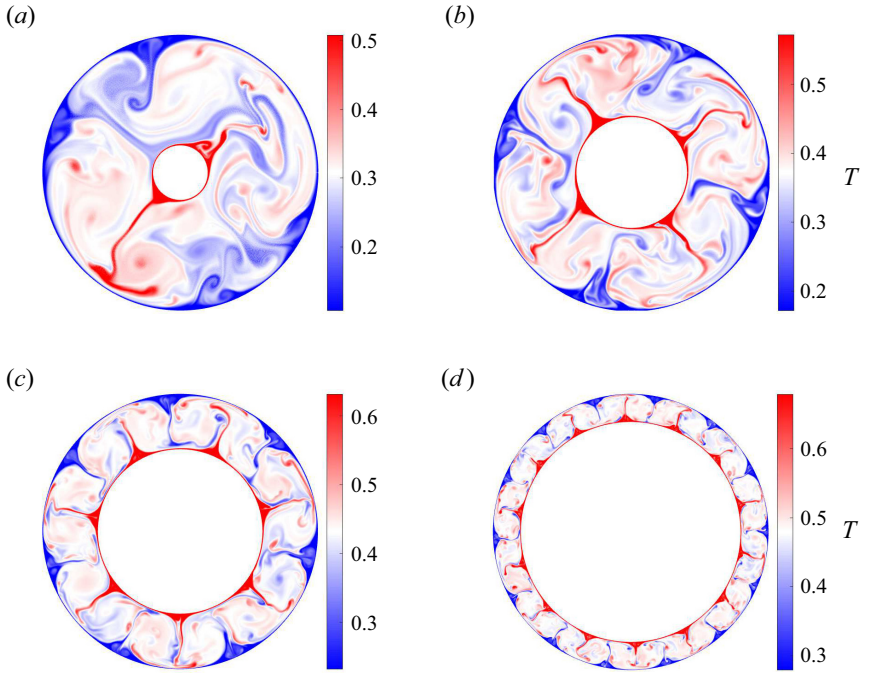

Figure 3. Instantaneous temperature fields for different η at $Ra = 10^8$: (*a*) $\eta = 0.2$, (*b*) $\eta = 0.4$, (*c*) $\eta = 0.6$, (*d*) $\eta = 0.8$.

where $\lambda_i(\lambda_o)$ is the TBL width near the inner (outer) wall, and $\Delta T_i(\Delta T_o)$ is the temperature drop within the corresponding TBLs. Moreover, based on our simulations (see figure 2) we conclude that, similar to planar RBC, the temperature drop across the shells occurs only in the BLs if the flow is turbulent (Ra is large). Hence, the following relation also holds true:

$$\Delta T_i + \Delta T_o = 1. \tag{4.2}$$

By the definition of Nu, evaluated at the walls, we have $Nu = r(\partial T/\partial r)\ln\eta$. From this, we obtain

$$\frac{\Delta T_i}{\lambda_i} \approx \frac{1-\eta}{\eta}\frac{Nu}{\ln\eta}, \tag{4.3}$$

$$\frac{\Delta T_o}{\lambda_o} \approx (1-\eta)\frac{Nu}{\ln\eta}. \tag{4.4}$$

Equations (4.3) and (4.4) combine to give (4.1). In order to quantify the variables ΔT_i, ΔT_o, λ_i and λ_o, (4.1), (4.2), (4.3) and (4.4) are not sufficient. Additional relations between the parameters are required.

4.1. *Wu & Libchaber assumption*

An asymmetric temperature field is also observed in planar NOB RBC (Wu & Libchaber 1991; Zhang, Childress & Libchaber 1997; Bodenschatz, Pesch & Ahlers 2000; Ahlers *et al.* 2006; Weiss, Emran & Shishkina 2024). Several authors have previously attempted to quantify the asymmetry of the temperature field due to the effects of NOB conditions on planar RBC systems (see Ahlers *et al.* 2006; Horn, Shishkina & Wagner 2013; Horn &

Shishkina 2014; Weiss *et al.* 2018; Yik, Valori & Weiss 2020). Possibly the simplest model was proposed in the seminal work of Wu & Libchaber (1991). Based on their experimental results, they inferred that in the central region, temperature fluctuation scales of the colder region are equal to that of the hotter region and obtained the following equality:

$$\theta_i \equiv \frac{\nu\kappa}{\alpha g_i {\lambda_i}^3} = \frac{\nu\kappa}{\alpha g_o {\lambda_o}^3} \equiv \theta_o. \tag{4.5}$$

Here, (g_i) and (g_o) are the gravitational accelerations at the inner and the outer TBLs, respectively. The proposed model could predict both the midpoint temperature and the heat transfer rate in an RBC cell with NOB effects. Wang *et al.* (2022) used this model to obtain relations between different BL parameters for RBC in a rotating cylindrical geometry. For the present flow configuration, it results in the following expressions:

$$\lambda_i = \frac{\eta \ln \eta}{(1+\eta^{2/3})(1-\eta)Nu}, \quad \Delta T_i = \frac{1}{1+\eta^{2/3}}, \tag{4.6a}$$

$$\lambda_o = \frac{\eta^{2/3} \ln \eta}{(1+\eta^{2/3})(1-\eta)Nu}, \quad \Delta T_o = \frac{\eta^{2/3}}{1+\eta^{2/3}}. \tag{4.6b}$$

Figure 4(*c*) shows the comparison of the analytical expression with the results from the present simulations. A significant deviation can be seen towards the lower η. Gastine *et al.* (2015) demonstrated that in spherical geometries, this model deviated from observed results under various gravity profiles, including uniform gravity. In the original study by Wu & Libchaber (1991), the model's validity was confirmed for $Pr \sim 1$, and Zhang *et al.* (1997) extended this to Pr values ranging from 300 to 7000. Thus, it appears that the Pr should not significantly impact the model's applicability. We hypothesize that the geometry of the container and in particular its curvature has a stronger impact. It influences the plume thickness along its path through the bulk, leading to changes in the temperature fluctuation scales and contributing to the observed deviations from the above model.

4.2. *Gastine et al. assumption*

Based on the disparity between the sizes of the plumes ejected from the inner and outer shells, Gastine *et al.* (2015) proposed that the average plume spacing in the inner and outer shells are equal. Their hypothesis was based on the observance that the plumes ejected from the outer BL are thicker than those ejected from the inner BL. To prove the hypothesis, they obtained probability distributions of the interplume area in both the inner and outer shells and found them to be overlapping. Furthermore, as the interplume area is proportional to the interplume spacing, they derived an expression for the interplume spacing in the inner (outer) shell as $l_i = \sqrt{\alpha g_i \Delta T_i {\lambda_i}^5/(\nu\kappa)}$ ($l_o = \sqrt{\alpha g_o \Delta T_o {\lambda_o}^5/(\nu\kappa)}$) which when equated leads to the following:

$$\sqrt{\frac{\alpha g_i \Delta T_i {\lambda_i}^5}{\nu\kappa}} = \sqrt{\frac{\alpha g_o \Delta T_o {\lambda_o}^5}{\nu\kappa}}. \tag{4.7}$$

Using (4.7) along with (4.1) and (4.2) we obtain that $\lambda_i/\lambda_o = \eta^{1/3}$. This leads to the same set of equations as (4.6*a*)–(4.6*b*). We have already seen that these equations do not concur with the results of present simulations. We conjecture that this might be due to the dominance of convective rolls in our set-up. Moreover, this model is based on geometrical constraints and does not depend on the gravity profile; it was efficient across various gravity profiles in Gastine *et al.* (2015). However, it has only been applied to the case of $Pr = 1$. Hence, it is unknown how it depends on Pr.

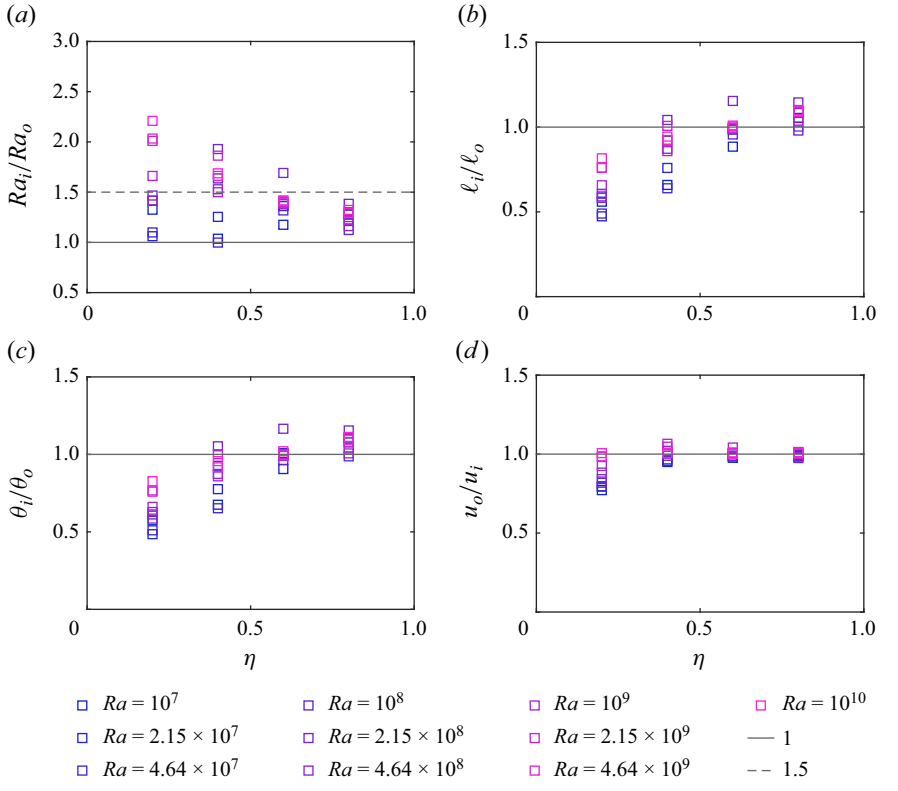

Figure 4. Comparison of the various scaling criteria with the present data. (*a*) Ratio of the BL *Ra* based on the argument of Jarvis (1993). (*b*) Ratio of average plume spacings in the inner and outer shells (Gastine *et al.* 2015). (*c*) Fluctuating temperature scales as defined in Wu & Libchaber (1991). (*d*) Ratio of the velocity scales of the inner and outer BLs.

4.3. *Jarvis assumption*

Based on the argument of marginal BL stability (Malkus 1954), Jarvis (1993) equate the BL Rayleigh numbers ($Ra_i = \alpha g_i \Delta T_i {\lambda_i}^3/(\nu\kappa)$ and $Ra_o = \alpha g_o \Delta T_o {\lambda_o}^3/(\nu\kappa)$) and obtain

$$\frac{\alpha g_i \Delta T_i {\lambda_i}^3}{\nu\kappa} = \frac{\alpha g_o \Delta T_o {\lambda_o}^3}{\nu\kappa}. \tag{4.8}$$

Equations (4.1), (4.2) and (4.8) lead to the following equations:

$$\lambda_i = \frac{\eta \ln \eta}{(1+\eta^{1/2})(1-\eta)Nu}, \quad \Delta T_i = \frac{1}{1+\eta^{1/2}}, \tag{4.9a}$$

$$\lambda_o = \frac{\eta^{1/2} \ln \eta}{(1+\eta^{1/2})(1-\eta)Nu}, \quad \Delta T_o = \frac{\eta^{1/2}}{1+\eta^{1/2}}. \tag{4.9b}$$

Figure 5(*a*) shows that the ratio of the TBLs follow $\lambda_i/\lambda_o \sim \eta^{1/2}$, indeed. Validation of the TBL thickness is further supported in figure 6(*b*). While the assumption $Ra_i = Ra_o$ can explain these observations, we find no solid physical justification for this assumption (see figure 4*a*). This model was originally validated for mantle convection with an infinite Prandtl number. However, since it is based on the marginal stability of the BLs, it is possible that the deviations between the model and our data are due to the lack of turbulence in the studied 2-D flows. Indeed, Gastine *et al.* (2015) found that this model

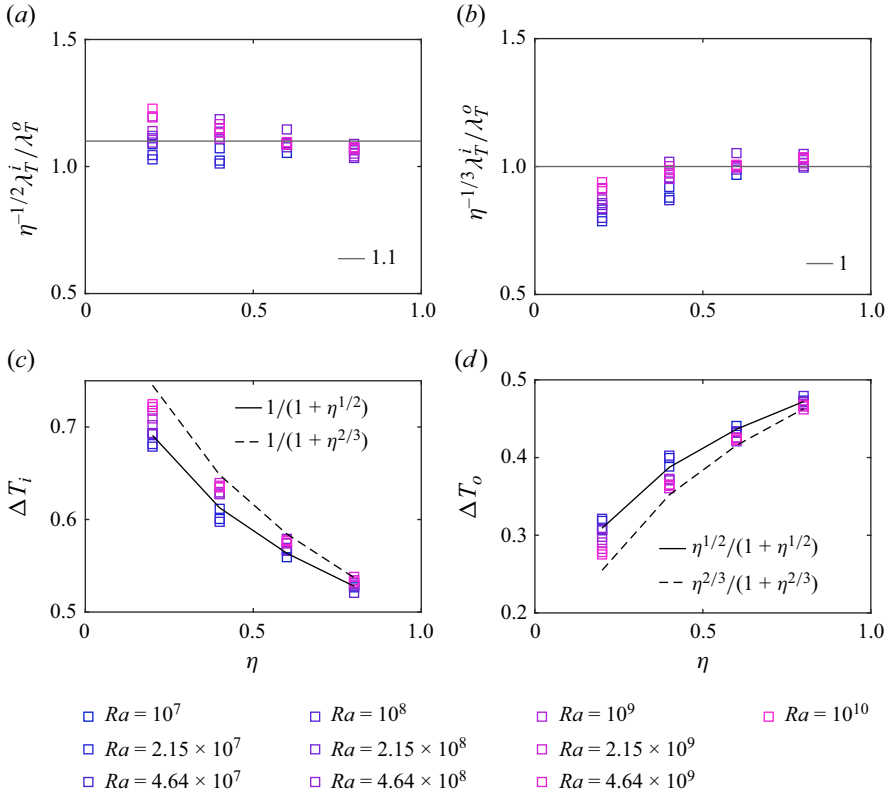

Figure 5. The TBL ratio compensated by (*a*) $\eta^{1/2}$ and (*b*) $\eta^{1/3}$. Temperature drop in the inner (*c*) and outer (*d*) TBL compared with the analytical results in (4.6*a*) and (4.6*b*) as well as (4.9*a*) and (4.9*b*).

did not match their simulation results for any of the gravity profiles they simulated. As a result, we refrain from adopting this argument and instead proceed with an alternative approach.

4.4. *Proposed model*

The flow is dominated by convective rolls which interact with the BLs and plumes. We assume that the viscous term of the temperature equation scales with the advective term at the BL width $u_\phi((1/r)(\partial T/\partial\phi)) \sim \kappa((1/r)(\partial/\partial r)(r(\partial T/\partial r)))$. Here, (r) and (ϕ) are the radial and azimuthal coordinate, respectively. This assumption is derived from the balance of the leading terms in the temperature equation (2.3). At the edge of the TBL, the magnitude of the azimuthal velocity component u_ϕ is significantly larger than the radial velocity component u_r. As a result, $u_\phi((1/r)(\partial T/\partial\phi)) \gg u_r(\partial T/\partial r)$. Similarly, for the diffusive term, the radial gradient of T dominates the azimuthal gradient. Therefore, $\kappa((1/r)(\partial/\partial r)(r(\partial T/\partial r))) \gg \kappa((1/r^2)(\partial^2 T/\partial\phi^2))$. Hence we define an advective length scale for the inner (outer) shells as $\mathcal{L}_i \sim r_i\,\mathrm{d}\phi$ ($\mathcal{L}_o \sim r_o\,\mathrm{d}\phi$) and take the BL thickness for the inner (outer) shell to be the vertical length scale. We define u_i (u_o) to be the velocity scale for the convective roll near the inner (outer) shell; we then obtain the following scaling relations:

$$\frac{u_i \Delta T_i}{\mathcal{L}_i} \sim \frac{\kappa\,\Delta T_i}{\lambda_i^2} \quad \text{and} \quad \frac{u_o \Delta T_o}{\mathcal{L}_o} \sim \frac{\kappa\,\Delta T_o}{\lambda_o^2}. \tag{4.10a,b}$$

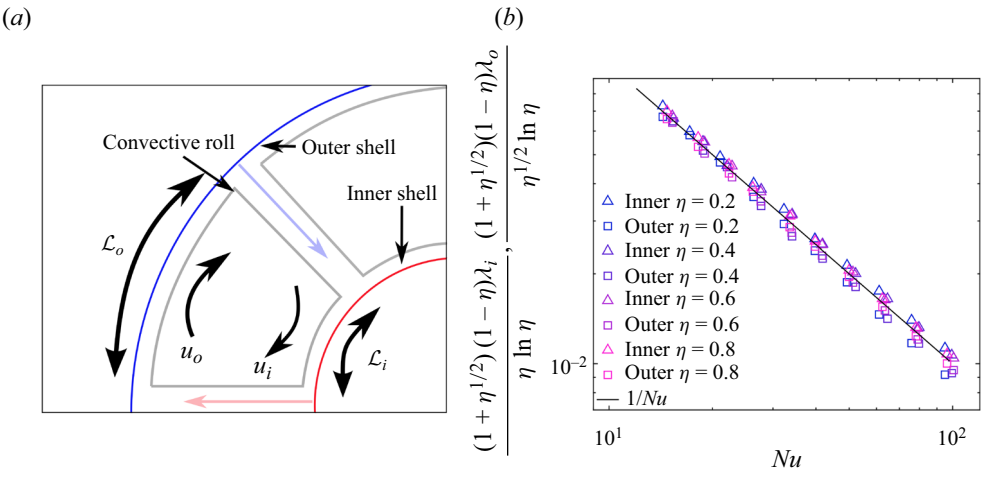

Figure 6. (*a*) A schematic of the velocity and length scales chosen to obtain scaling arguments. (*b*) Comparison of the normalized TBL width with the analytical result, (4.9*a*) and (4.9*b*).

Therefore,

$$\frac{u_i}{u_o} \sim \frac{\mathcal{L}_i \lambda_o^2}{\mathcal{L}_o \lambda_i^2}, \tag{4.11}$$

where $\mathcal{L}_i/\mathcal{L}_o = \eta$, see figure 6. We further propose that the velocity scales of the convective roll near the inner and outer shells are equal, i.e. $u_i = u_o$ (see figure 4*d*). The ratio u_i/u_o shown in figure 4(*d*) is that of the peaks of the root-mean-squared velocity near the inner and outer shell. The equality $u_i = u_o$ can be justified as the 2-D nature of the flow ensures the azimuthal mass flux near the outer shell equals that towards the inner shell, and as the convective roll is symmetrically placed along the radial direction the velocity scales should be equal. Figure 4(*d*) shows that at lower η, there is a higher scatter of the ratio of u_i and u_o and of the ratio of the TBL thickness (figure 5*a*). This might be attributed to the breaking of the cold plume at lower radius ratios as discussed in § 3. Thus from (4.11), $u_i = u_o$ and $\mathcal{L}_i/\mathcal{L}_o = \eta$ we conclude that $\lambda_i/\lambda_o \sim \eta^{1/2}$, which is supported by our DNS results, see figure 5(*a*). This physics-based model can also lead to the derivations of (4.9*a*) and (4.9*b*).

5. Conclusion

In this study, we derived scaling laws for the TBL width ratio in RBC within a 2-D annulus, focusing on radius ratios ranging from 0.2 to 0.8 and Rayleigh numbers (Ra) from 10^7 to 10^{10}. The system features a gravity profile $g \propto 1/r$ with a fixed $Pr = 1$. We observed an asymmetry in the TBL widths between the inner and outer shells, consistent with previous studies. However, existing scaling laws failed to quantify this asymmetry. To address this, we proposed a new scaling argument based on the assumptions of the isothermal bulk and constant velocity along the path of all large-scale convection rolls that develop in the annulus RBC. This new scaling successfully predicted the temperature drops and TBL widths across the parameter range studied.

Funding. The authors acknowledge the financial support from the Max Planck Society, Germany, and the German Research Foundation (DFG), Sh405/20, Sh405/22, 521319293, 540422505 and 550262949. The authors gratefully acknowledge the computing time provided to them on the high-performance computer Lichtenberg at the NHR Centers NHR4CES at TU Darmstadt, funded by the Federal Ministry of Education

and Research, Germany, and the state governments participating on the basis of the resolutions of the GWK for national high-performance computing at universities, on the HPC systems of Max Planck Computing and Data Facility (MPCDF), on the HoreKa supercomputer funded by the Ministry of Science, Research and the Arts Baden-Württemberg and by the Federal Ministry of Education and Research, and on the GCS Supercomputer SuperMUC-NG at Leibniz Supercomputing Centre (LRZ). A.B. conducted the work in this paper in the framework of the International Max-Planck Research School (IMPRS) for Solar System Science at the University of Göttingen.

Declaration of interests. The authors report no conflict of interest.

Author ORCIDs.
Abhiroop Bhadra https://orcid.org/0000-0001-5168-966X;
Olga Shishkina https://orcid.org/0000-0002-6773-6464;
Xiaojue Zhu https://orcid.org/0000-0002-7878-0655.

Appendix

Table 1 lists the simulation data.

Ra	Nu	$Nu_{error\%}$	$N^U_{BL,i}$	$N^U_{BL,o}$	$N^T_{BL,i}$	$N^T_{BL,o}$	$\frac{r\Delta\theta_{max}}{\eta_K}$	$\frac{\Delta r_{max}}{\eta_K}$	τ_{avg}	$N_r \times N_\theta$
					$\eta = 0.2$					
1×10^7	14.33	0.18	10	16	17	26	0.68	0.57	6039	256×1152
2.15×10^7	17.16	0.20	9	15	14	23	0.86	0.72	3430	256×1152
4.64×10^7	21.04	0.19	9	15	14	22	1.1	0.95	3397	256×1152
1×10^8	26.35	0.21	8	13	12	18	1.46	1.25	3340	256×1152
2.15×10^8	32.28	0.34	7	11	11	16	1.92	1.64	2921	256×1152
4.64×10^8	39.73	0.04	9	17	15	25	1.25	1.04	929	512×2304
1×10^9	49.27	0.3	9	16	14	22	1.61	1.35	557	512×2304
2.15×10^9	61.11	0.13	8	14	14	20	2.08	1.77	592	512×2304
4.64×10^9	75.40	2	9	16	15	22	1.78	1.50	1534	768×3456
1×10^9	94.56	1.43	16	27	24	35	1.72	1.50	500	1024×4608
					$\eta = 0.4$					
1×10^7	15.4	0.16	12	15	19	24	0.57	0.55	3342	256×1800
2.15×10^7	18.77	0.2	11	13	17	21	0.73	0.70	4256	256×1800
4.64×10^7	22.06	0.2	10	12	15	19	0.93	0.91	3791	256×1800
1×10^8	27.71	0.3	8	10	12	14	1.20	1.16	3788	256×1800
2.15×10^8	34.09	0.3	7	9	11	12	1.56	1.52	3442	256×1800
4.64×10^8	41.81	0.28	12	16	19	23	1.02	1	923	512×3600
1×10^9	51.87	0.97	10	14	16	19	1.33	1.29	1002	512×3600
2.15×10^9	64.61	0.49	9	12	14	15	1.72	1.67	777	512×3600
4.64×10^9	79.54	1.71	12	16	18	21	1.48	1.45	1149	768×5400
1×10^{10}	99.01	2.8	21	27	29	34	1.42	1.45	327	1024×7200
					$\eta = 0.6$					
1×10^7	15.28	0.13	13	15	21	23	0.53	0.48	815	256×3072
2.15×10^7	18.96	0.21	11	12	19	19	0.68	0.61	499	256×3072
4.64×10^7	22.80	0.21	10	11	16	17	0.87	0.78	499	256×3072
1×10^8	27.72	0.35	9	9	14	14	1.1	1	1023	256×3072
2.15×10^8	33.98	0.37	8	9	13	12	1.45	1.31	499	256×3072

Table 1. For caption see next page.

Ra	Nu	$Nu_{error\%}$	$N^U_{BL,i}$	$N^U_{BL,o}$	$N^T_{BL,i}$	$N^T_{BL,o}$	$\frac{r\Delta\theta_{max}}{\eta_K}$	$\frac{\Delta r_{max}}{\eta_K}$	τ_{avg}	$N_r \times N_\theta$
4.64×10^8	41.48	0.34	13	15	21	22	0.96	0.86	1100	512×6144
1×10^9	51.48	0.83	12	14	18	19	1.24	1.12	2722	512×6144
2.15×10^9	63.28	0.87	10	11	15	16	1.61	1.45	2482	512×6144
4.64×10^9	80.02	1.84	14	16	20	21	1.4	1.24	606	768×9216
1×10^9	99.28	0.61	23	26	31	33	1.42	1.22	130	$1024 \times 12\,288$
					$\eta = 0.8$					
1×10^7	14.74	0.17	14	14	23	22	0.41	0.51	1208	256×6912
2.15×10^7	18.16	0.18	13	12	20	19	0.52	0.66	1311	256×6912
4.64×10^7	22.33	0.25	11	11	17	17	0.67	0.83	1245	256×6912
1×10^8	26.19	0.35	9	9	15	14	0.86	1.06	1131	256×6912
2.15×10^8	33.54	0.40	9	8	13	12	1.12	1.39	1030	256×6912
4.64×10^8	39.72	0.61	15	15	23	22	0.74	0.92	1406	$512 \times 13\,824$
1×10^9	49.71	1.01	13	13	19	18	0.96	1.19	1199	$512 \times 13\,824$
2.15×10^9	62.08	1.35	11	11	16	15	1.25	1.55	1032	$512 \times 13\,824$
4.69×10^9	77.25	0.33	15	15	21	20	1.07	1.35	1707	$768 \times 5184*$
1×10^{10}	95.78	1.97	25	25	34	33	1.03	1.35	525	$1024 \times 6912*$

Table 1. Simulation details. Here, Ra is the Rayleigh number; Nu is the average of the Nusselt numbers computed from the thermal dissipation, kinetic dissipation and inner and outer shell heat flux; $Nu_{error\%}$ is the percentage of relative error between the maximum and minimum of the previously mentioned Nu; $N^U_{BL,i/o}$ is the number of grid points in the inner/outer UBL; $N^T_{BL,i/o}$ is the number of grid points in the inner/outer TBL; $r\Delta\theta_{max}/\eta_K$ and $\Delta r_{max}/\eta_K$ is the ratio of the maximum grid spacing in the azimuthal and radial direction, respectively, to the global Kolmogorov length scale in the bulk region of the flow; τ_{avg} is the averaging time; and N_r and N_θ represent the resolution of the grid in radial and azimuthal directions. At $\eta = 0.8$ for $Ra = 4.69 \times 10^9$ and $Ra = 1 \times 10^{10}$ (indicated by an asterisk in the last column), only a quarter of the cylinder is simulated.

References

Ahlers, G., Brown, E., Araujo, F.F., Funfschilling, D., Grossmann, S. & Lohse, D. 2006 Non-Oberbeck–Boussinesq effects in strongly turbulent Rayleigh–Bénard convection. *J. Fluid Mech.* **569**, 409–445.

Ahlers, G., Grossmann, S. & Lohse, D. 2009 Heat transfer and large scale dynamics in turbulent Rayleigh–Bénard convection. *Rev. Mod. Phys.* **81** (2), 503.

Bodenschatz, E., Pesch, W. & Ahlers, G. 2000 Recent developments in Rayleigh–Bénard convection. *Annu. Rev. Fluid Mech.* **32** (1), 709–778.

Chillà, F. & Schumacher, J. 2012 New perspectives in turbulent Rayleigh–Bénard convection. *Eur. Phys. J.* E **35**, 1–25.

Ching, E.S.C., Guo, H., Shang, X.-D., Tong, P. & Xia, K.-Q. 2004 Extraction of plumes in turbulent thermal convection. *Phys. Rev. Lett.* **93** (12), 124501.

Christensen, U.R. 2001 Zonal flow driven by deep convection in the major planets. *Geophys. Res. Lett.* **28** (13), 2553–2556.

Christensen, U.R. & Wicht, J. 2008 Models of magnetic field generation in partly stable planetary cores: applications to Mercury and Saturn. *Icarus* **196** (1), 16–34.

Deschamps, F., Tackley, P.J. & Nakagawa, T. 2010 Temperature and heat flux scalings for isoviscous thermal convection in spherical geometry. *Geophys. J. Intl* **182** (1), 137–154.

Gastine, T., Wicht, J. & Aurnou, J.M. 2015 Turbulent Rayleigh–Bénard convection in spherical shells. *J. Fluid Mech.* **778**, 721–764.

Hirose, S., Blaes, O., Krolik, J.H., Coleman, M.S.B. & Sano, T. 2014 Convection causes enhanced magnetic turbulence in accretion disks in outburst. *Astrophys. J.* **787** (1), 1.

Horn, S. & Shishkina, O. 2014 Rotating non-Oberbeck–Boussinesq Rayleigh–Bénard convection in water. *Phys. Fluids* **26** (5), 055111.

HORN, S., SHISHKINA, O. & WAGNER, C. 2013 On non-Oberbeck–Boussinesq effects in three-dimensional Rayleigh–Bénard convection in glycerol. *J. Fluid Mech.* **724**, 175–202.

HOTTA, H. & KUSANO, K. 2021 Solar differential rotation reproduced with high-resolution simulation. *Nat. Astron.* **5** (11), 1100–1102.

JARVIS, G.T. 1993 Effects of curvature on two-dimensional models of mantle convection: cylindrical polar coordinates. *J. Geophys. Res.: Sol. Ea.* **98** (B3), 4477–4485.

JIANG, H., WANG, D., LIU, S. & SUN, C. 2022 Experimental evidence for the existence of the ultimate regime in rapidly rotating turbulent thermal convection. *Phys. Rev. Lett.* **129** (20), 204502.

JIANG, H., ZHU, X., WANG, D., HUISMAN, S.G. & SUN, C. 2020 Supergravitational turbulent thermal convection. *Sci. Adv.* **6** (40), eabb8676.

KLAHR, H. 2006 Thermal convection in accretion disks. *Proc. Intl Astron. Union* **2** (S239), 405–416.

LOHSE, D. & SHISHKINA, O. 2024 Ultimate Rayleigh–Bénard turbulence. *Rev. Mod. Phys.* **96** (3), 035001.

LOHSE, D. & XIA, K.-Q. 2010 Small-scale properties of turbulent Rayleigh–Bénard convection. *Annu. Rev. Fluid Mech.* **42** (1), 335–364.

MALKUS, W.V.R. 1954 The heat transport and spectrum of thermal turbulence. *Proc. R. Soc. Lond.* A **225** (1161), 196–212.

SAMUEL, H., BALLMER, M.D., PADOVAN, S., TOSI, N., RIVOLDINI, A. & PLESA, A.-C. 2021 The thermo-chemical evolution of Mars with a strongly stratified mantle. *J. Geophys. Res.: Planet.* **126** (4), e2020JE006613.

SCHUBERT, G. & ZEBIB, A. 1980 Thermal convection of an internally heated infinite Prandtl number fluid in a spherical shell. *Geophys. Astrophys. Fluid Dyn.* **15** (1), 65–90.

SHARPE, H.N. & PELTIER, W.R. 1978 Parameterized mantle convection and the Earth's thermal history. *Geophys. Res. Lett.* **5** (9), 737–740.

SHISHKINA, O. 2021 Rayleigh–Bénard convection: the container shape matters. *Phys. Rev. Fluids* **6** (9), 090502.

SHISHKINA, O., STEVENS, R.J.A.M., GROSSMANN, S. & LOHSE, D. 2010 Boundary layer structure in turbulent thermal convection and its consequences for the required numerical resolution. *New J. Phys.* **12** (7), 075022.

TEED, R.J. & LATTER, H.N. 2021 Axisymmetric simulations of the convective overstability in protoplanetary discs. *Mon. Not. R. Astron. Soc.* **507** (4), 5523–5541.

TILGNER, A. 1996 High-Rayleigh-number convection in spherical shells. *Phys. Rev.* E **53** (5), 4847.

VAN DER POEL, E.P., OSTILLA-MÓNICO, R., DONNERS, J. & VERZICCO, R. 2015 A pencil distributed finite difference code for strongly turbulent wall-bounded flows. *Comput. Fluids* **116**, 10–16.

VANGELOV, V.I. & JARVIS, G.T. 1994 Geometrical effects of curvature in axisymmetric spherical models of mantle convection. *J. Geophys. Res.: Sol. Ea.* **99** (B5), 9345–9358.

VASIL, G.M., JULIEN, K. & FEATHERSTONE, N.A. 2021 Rotation suppresses giant-scale solar convection. *Proc. Natl Acad. Sci. USA* **118** (31), e2022518118.

VERZICCO, R. & ORLANDI, P. 1996 A finite-difference scheme for three-dimensional incompressible flows in cylindrical coordinates. *J. Comput. Phys.* **123** (2), 402–414.

WANG, D., JIANG, H., LIU, S., ZHU, X. & SUN, C. 2022 Effects of radius ratio on annular centrifugal Rayleigh–Bénard convection. *J. Fluid Mech.* **930**, A19.

WANG, D., LIU, J., ZHOU, Q. & SUN, C. 2023 Statistics of temperature and velocity fluctuations in supergravitational convective turbulence. *Acta Mechanica Sin.* **39** (4), 122387.

WEISS, S., EMRAN, M.S. & SHISHKINA, O. 2024 What Rayleigh numbers are achievable under Oberbeck–Boussinesq conditions? *J. Fluid Mech.* **986**, R2.

WEISS, S., HE, X., AHLERS, G., BODENSCHATZ, E. & SHISHKINA, O. 2018 Bulk temperature and heat transport in turbulent Rayleigh–Bénard convection of fluids with temperature-dependent properties. *J. Fluid Mech.* **851**, 374–390.

WU, X.-Z. & LIBCHABER, A. 1991 Non-Boussinesq effects in free thermal convection. *Phys. Rev.* A **43** (6), 2833.

YAO, Z., EMRAN, M.S., TEIMURAZOV, A. & SHISHKINA, O. 2025 Direct numerical simulations of centrifugal convection: from gravitational to centrifugal buoyancy dominance. *Intl J. Heat Mass Transfer* **236**, 126314.

YIK, H., VALORI, V. & WEISS, S. 2020 Turbulent Rayleigh–Bénard convection under strong non-Oberbeck–Boussinesq conditions. *Phys. Rev. Fluids* **5** (10), 103502.

ZEBIB, A., SCHUBERT, G., DEIN, J.L. & PALIWAL, R.C. 1983 Character and stability of axisymmetric thermal convection in spheres and spherical shells. *Geophys. Astrophys. Fluid Dyn.* **23** (1), 1–42.

ZHANG, J., CHILDRESS, S. & LIBCHABER, A. 1997 Non-Boussinesq effect: thermal convection with broken symmetry. *Phys. Fluids* **9** (4), 1034–1042.

ZHONG, J., LI, J. & SUN, C. 2024 Effect of radius ratio on the sheared annular centrifugal turbulent convection. *J. Fluid Mech.* **992**, A16.

ZHONG, J., WANG, D. & SUN, C. 2023 From sheared annular centrifugal Rayleigh–Bénard convection to radially heated Taylor–Couette flow: exploring the impact of buoyancy and shear on heat transfer and flow structure. *J. Fluid Mech.* **972**, A29.

ZHU, X., MATHAI, V., STEVENS, R.J.A.M., VERZICCO, R. & LOHSE, D. 2018*a* Transition to the ultimate regime in two-dimensional Rayleigh–Bénard convection. *Phys. Rev. Lett.* **120** (14), 144502.

ZHU, X., *et al*. 2018*b* AFiD-GPU: a versatile Navier–Stokes solver for wall-bounded turbulent flows on GPU clusters. *Comput. Phys. Commun.* **229**, 199–210.